Simulation of the influence of alloying elements on the characteristics of the formation of vacuum-arc nitride coatings

N.V. Pinchuk [1,2], V.V. Subbotina[1], O.S. Terletskyi[1], I.M. Kolupaiev [1], M.M. Tkachuk[1,2], S.V. Hryhorieva[1]

[1] National Technical University «Kharkiv Polytechnic Institute», Kharkiv, Ukraine
[2] Karlstad University, Karlstad, Sweden

An analysis of trends in the interaction of elements of the Periodic Table was carried out and the results obtained were compared with a model material (namely with a TiN coating); predictions were made for structure formation in vacuum-arc nitride coatings and modeling of the properties of the final coating depending on the composition and deposition conditions This made it possible to explain changes in structural characteristics and mechanical properties in the presence of weaker and/or stronger nitride-forming elements in nitride coatings. Under all deposition conditions and different elemental compositions, single-phase crystalline coatings were obtained. The addition of Mo to the coating increases the lattice period of TiMoN. It was established that the high-entropy coatings (TiVZrNbHf)N and (TiVZrNbHfTa)N are single-phase with an fcc lattice. The high entropy of the system prevents the formation of intermetallic compounds. The coatings are polycrystalline with a crystallite size of 20-23 nm. It has been established that high-entropy coatings obtained at a nitrogen atmosphere pressure of 0.26 Pa and a constant bias potential of −200 V have the highest hardness value of 53–55 GPa. The theoretical model used to analyze the characteristics of high-entropy alloys and nitride coatings based on them has been confirmed experimentally.

Keywords: Coatings, High-entropy alloys (HEA), Structural engineering, Alloying, Multi-component nitrides, Texture.

Моделювання впливу легуючих елементів на особливості формування вакуумно-дугових нітридних окриттів.*Н.В. Пінчук, В.В. Субботіна, О.С. Терлецький, І.М. Колупаєв,М.М. Ткачук, С.В. Григор'єва*

Завдяки аналізу тенденцій взаємодії елементів періодичної таблиці та порівнюючи отримані результати з модельним матеріалом (а саме покриття TiN), було зроблено прогнози стосовно структуроутворення у вакуумно-дугових нітридних покриттях та моделювання стосовно властивостей кінцевого покриття в залежності від складу та умов осадження. Розуміння цього дозволило, в свою чергу, пояснити зміни в структурних характеристиках та механічних властивостях при наявності більш слабких та/або більш сильних нітридоутворюючих елементів у нітридних покриттях. При усіх умовах осадження та різній композиції елементів отримані однофазні кристалічні покриття. Додавання Mo у покриття збільшує період решітки TiMoN. Встановлено, що високоентропійні покриття (TiVZrNbHf)N та (TiVZrNbHfTa)N характеризуються однофазним станом з ГЦК решіткою. Висока ентропія системи запобігає формуванню інтерметалічних сполук. Покриття мають структуру з розміром кристалітів 20-23 нм. Встановлено, що найбільше значення твердісті мають високоентропійні покриття, отримані при тиску азотної атмосфери 0.26 Па і постійному потенціалі зміщення −200 В та складають 53– 55 ГПа. Теоретична модель, використана для аналізу характеристик високоентропійних сплавів та нітридних покриттів на їх основі, підтверджена експериментально.

1. Introduction

Issues of modification (alloying) of the surface of a solid body play an important and sometimes decisive role in mechanical engineering. Among all nano-oriented surface treatment technologies, ion-vacuum PVD (Physical Vapor Deposition) and CVD (Chemical Varour Deposition) technologies are the most promising today [1]. The composition and properties of the obtained coatings largely depend on the technology of their deposition. To this day, technologies for applying wear-resistant coatings, such as TiN, TiCN, TiAlN, etc., are relevant. The results of fundamental research of nanocrystalline films and coatings are presented in many works [2-10].

Coatings and films of titanium nitride (TiN) have been known for a long time, but they do not lose their relevance, as they have a unique combination of properties: high values of hardness, wear resistance, melting temperature, as well as chemical inertness and thermodynamic stability, high electrical and thermal conductivity [11, 12]. These qualities have determined a wide range of their application as protective, corrosion-resistant, decorative and barrier layers – in various fields of mechanical engineering, electronics, and medicine [13-15]. In order to achieve the best operational characteristics of coatings and films, it is necessary to improve the methods of their production. Modern protective coatings must meet high requirements and combine high physical, mechanical and operational characteristics to ensure reliable operation and increase the service life of tools, parts, mechanisms and various products.

The operational properties of strengthening coatings are largely determined by their structural and phase state, the level of internal stresses, structural defects, and crystallite sizes. Binary titanium nitride (TiN) layers are ideal for protective coatings on metalworking tools, piston engines, turbine blades, etc. But due to the ever-increasing requirements for thin-film materials, titanium nitride coatings are being replaced by multicomponent systems based on them, the characteristics of which are many times greater than those of the traditional TiN coating.

2. Experimental

All samples were obtained on the modernized Bulat-6 installation [16]. During vacuum-arc deposition, the following cathode materials were used: titanium VT 1-0; TiMo alloy; Ti-V-Zr-Nb-Hf and Ti-V-Zr-Nb-Hf-Ta castings produced by the method of vacuum-arc melting in an atmosphere of high-purity argon [17]. The elements that make up high-entropy alloys (HEA) are chosen taking into account the fact that they form a solid solution. According to the literature, remelted high-entropy equiatomic alloys are solid solutions based on a bcc lattice, which can be formed on the basis of certain groups of elements [17]. The selection and ratio of their concentrations in the alloy is carried out in such a way as to achieve high values of the entropy of mixing, due to which the free energy of the alloy decreases according to the Gibbs equation. Melting was carried out with a non-consumable tungsten electrode in a water-cooled copper mold. The resulting castings were remelted for 6-7 times to homogenize the composition. Nitrogen of special purity (99.999%) was used as the active gas in the working chamber during deposition. Polished samples of 20x20x3 mm stainless steel 12Cr18Ni9Ti (AISI 321) were used as substrates. Nitrogen pressure (p_{N2}) in the vacuum chamber during deposition was 0.26 Pa...0.66 Pa. The value of the constant bias potential (U_c) was in the range from –5...8 V to –200 V, the deposition rate was 1.5 nm/s, and the coating thickness was 7-10 μm. The duration of the deposition process was from 1 to 2 hours.

Phase and structural studies were carried out on a "DRON-3M" type apparatus in filtered copper radiation according to the Bragg-Brentano θ-2θ-scanning scheme. The measurements were carried out in the angle range $2\theta = (30 - 80)$ °. All diffraction peaks from the most closely packed planes fall into this angular range. Scanning step θ = 0.1°.

The substructural characteristics were analyzed by the method of approximating the shape of two orders of diffraction reflections from the planes of the crystal lattice using the Cauchy approximation function [18]. To study the stress-strain state, the method of multiple oblique recordings ("a-sin²ψ"-method) and the method of crystal groups were used [19, 20]. In X-ray methods, the scale of deformation measurement is the interplanar distance d. The relative error in determining the reflection angle is proportional to cot θ, so it decreases with increasing angle θ. Therefore, to more accurately determine the interplanar distance, reflections at large angles are chosen. In addition, to determine elastic macrostrains, reflections from the (420), (422) and (511) planes at angles ψ corresponding to the texture planes were used. Microindentation was performed on a "Micron-gamma" device [21, 22] at room temperature (load up to 0.5 N) with a Berkovich diamond pyramid.

The X-ray fluorescence method (XRF) was used to determine the elemental composition. The measurements were carried out on a SPRUT spectrometer (Ukraine, State Standard
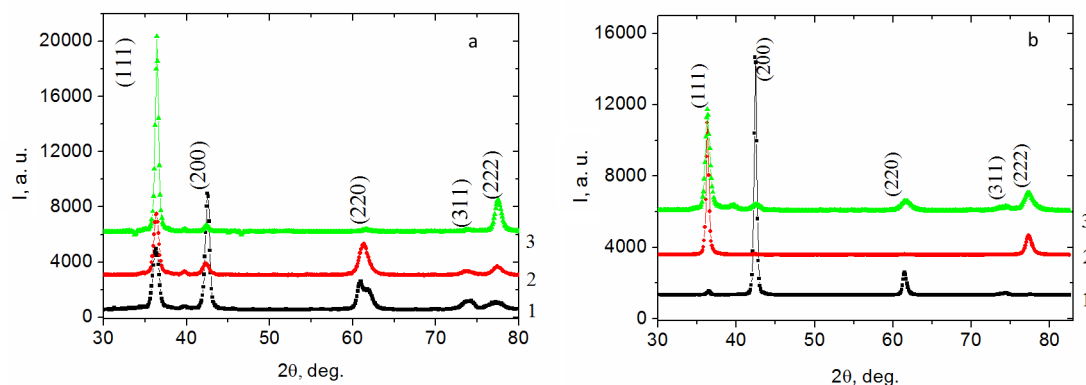
Fig. 1. XRD patterns of TiN coatings obtained at $p_N = 0.26$ Pa (a) and $p_N = 0.66$ Pa (b): $1 - U_c = (-5...-8)$ V; $2 - U_c = -90$ V; $3 - U_c = -200$ V

of Ukraine No. U703-96). The primary excitation radiation of an X-ray tube with a transmission Ag anode at an excitation voltage of 42 kV was used. The method is based on the dependence of the intensity of X-ray fluorescence on the concentration of the element in the sample.

3. Results and discussion

3.1. Model coatings

TiN was chosen as a model material and the influence of deposition conditions on the features of structure formation and properties of these coatings was analyzed.

The sections of diffraction spectra were obtained from coatings deposited at different working pressures of 0.26 Pa (Fig. 1 a) and 0.66 Pa (Fig. 1 b) at different values of constant negative bias potentials (U_c) ((from 0 V, which more closely corresponds to "floating", i.e. (-5...-8) V, –90 V and –200 V) applied to the substrate during deposition.

It can be seen that for two pressures in the entire range of constant bias potentials, the formation of a TiN phase with a cubic crystal lattice (structural type NaCl, JCPDS 38-1420) occurs. In the case of a lower pressure of the working atmosphere of 0.26 Pa, without a special supply of potential to the substrate, practically non-textured coatings are formed (Fig. 1a, line 1), as evidenced by the entire spectrum of diffraction peaks with characteristic intensity for different planes of the TiN lattice. Applying a bias potential of –90 V leads to the formation of a bitextured state with [111] and [110] axes in the case of low pressure during deposition (Fig. 1a, line 2).

At a higher p_N pressure (0.66 Pa) and a "floating" potential, when the average energy of titanium atoms practically does not increase compared to the average statistical distribution of sputtered atoms, coatings are formed with the texture axis [100] (Fig. 1 b, line 1). Applying a negative bias potential (–90 V and –200 V) leads to preferential growth of crystallites along the [111] axis, as can be seen in Fig. 1b (lines 2 and 3) by a significant increase in the intensity of peaks (111) and (222).

The elastic stress-strain state was analyzed by the "sin²ψ method" and its modification (the "crystal group" method [18, 20] with a clearly expressed texture in the coatings). At a lower operating pressure of 0.26 Pa, higher compressive macrostrains (ε) occur, reaching the value $\varepsilon = -2.1\%$, especially at $U_c = -200$ V, with a larger lattice period in the unstressed section compared to the table value ($a_0 = 0.4244$ nm (PDF No. 87-0629)) (Table 1). At the same time, the compressive stress (o) in the coating reached a maximum of –6.5 GPa.

The analysis of substructural characteristics (microstrain and size of crystallites) was carried out by the method of approximating the shape of diffraction reflections of two orders from the planes of the crystal lattice. At a working atmosphere pressure of 0.26 Pa, an increase in Uc leads to an increase in the average crystallite size with a somewhat non-monotonic change in microstrain (Table 1). The greatest microstrains are achieved when using a bias potential in the range of values (-100...-150) V, which correlates with an increase in the lattice period in the unstressed section (Table 1). Accordingly, it can be assumed that the increase in microstrain (i.e., strain of the 2nd kind, balanced inside the grain-crystallite) is due to the higher density of atoms in the lattices and the high compressive stresses observed at the same time (Table 1). It is also clear that an increase in operating pressure to 0.66 Pa leads to the same dependence of L and $<\varepsilon>$ on the value of the constant potential.

The features of the formation of single-component TiN coatings were analyzed, taking into account the influence of deposition conditions

Table 1 – Macrostrains (ε), lattice period (a_0), crystallite size (L) and microstrains (<ε>) of TiN coatings at different constant bias potentials and nitrogen atmosphere pressure

U_c, V	p_N = 0.26 Pa				p_N = 0.66 Pa			
	ε , %	a_0, nm	L, nm	(<ε>, %	ε , %	a_0, nm	L, nm	(<ε>, %
-5...-8	-1.3	0.42539	31	0.28	-0.1	0.42634	24	0.12
-90	-1.4	0.4277	48	0.41	-1.82	0.42863	118	0.62
-200	-2.1	0.42663	53	0.37	-1.95	0.42863	91	0.7

* $a_{0\,tabl}$ = 0.4244 nm (PDF # 87-0629)

Table 2 – Deposition conditions of TiMoN coatings and elemental composition of TiMo targets

Sample No	Coating	Deposition conditions		Elemental composition of targets	
		U_c, V	p_N ,Pa	Ti, at.%	Mo, at.%
1271	TiMoN	-70	0.53	86.7	13.3
1270	TiMoN	-200	0.53	86.52	13.48

on the formation of the structure and phase composition. It was established that in all deposition modes, a single-phase state with an fcc lattice is formed. An increase in the constant potential from –5...-8 V to –200 V promotes the formation of textured coatings with the [111] texture axis, as well as an increase in the size of crystallites due to heating of the substrate, which causes intense heating of the coating at the crystallization front during the deposition process. As the bias potential increases, the collision energy of the plasma flow with the substrate increases, as well as the radius of the temperature peak, i.e., the time required to cool the collision region to the initial temperature increases. If the temperature peak lasts long enough, it provides the time necessary for significant atomic shifts and relaxations corresponding to local annealing. Thus, such collisions at high potential values generating temperature peaks with a lifetime exceeding the stress relaxation time of the processed material, can lead to an increase in crystallite sizes. The residual macrostresses present in all coatings were of a compressive nature.

3.2. TiMoN coatings

The next stage of the research is the modeling of the influence of alloying elements included in the target on the features of the formation of TiN-based coatings. Since significant differences in the formation of the preferential orientation (transition from [100] to [111] texture) of model TiN coatings were found when the constant potential changed from (-5...-8) V to –90 V, there was a need to study the effect of Mo on the formation of preferential orientation in TiMoN coatings. Therefore, TiMoN coatings were obtained at different values of the constant potential U_c (–70 V and –200 V) at the
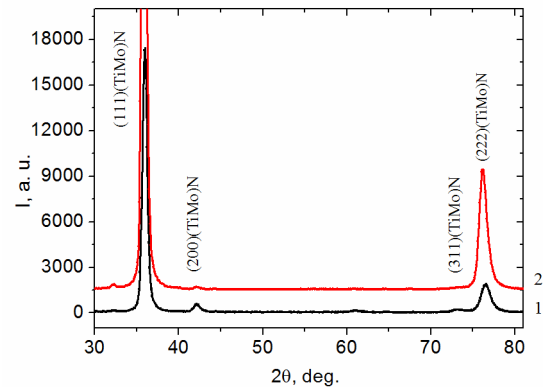

Fig. 2. XRD patterns of TiMoN coatings obtained at p_N = 0.53 Pa: 1 – U_c = –70 V; 2 – U_c = –200 V

pressure of a nitrogen atmosphere of 0.53 Pa. The deposition conditions and elemental composition of targets are given in Table 2. Fig. 2 shows sections of X-ray diffraction spectra from these coatings.

It can be seen that in the TiMoN coatings, the same type of crystal lattice of fcc type (structural type B1-NaCl) is formed. As U_c increases, a texture with the [111] axis is formed and at the same time its perfection increases (Fig. 2, line 2); that is, the relative intensity from the (111) lines increases in comparison with the table values for the TiN (ICDD PDF No. 00-087-0629) and MoN (ICDD PDF No. 01-079-5757) phases. The same trend was observed for TiN coatings (Fig. 1 b, lines 2, 3).

An increase in the width of diffraction maxima indicates the formation of nanostructured coatings. The crystallites were found to have an internal developed substructure, with an average size (L) of 14.3 nm and 16 nm, microstrain (<ε>) of 0.55% and 0.42% in samples 1271 and

1270, respectively. The lattice parameter (a) varies in the range of 0.4330-0.4337 nm depending on the elemental composition of the coatings (Table 2). The shift in the position of the peaks on the diffraction patterns towards smaller angles is explained by differences in the crystal lattice parameter a at different elemental composition (the presence of Ti atoms leads to a decrease in the lattice parameter [23]).

Thus, the introduction of Mo into the composition of the coating does not change the structural state of the coating, while the tendency to form highly textured coatings with a pronounced texture remains [111]; such changes are especially noticeable in the increased values of the constant bias potential up to –200 V. In turn, Mo contributes to an increase in the lattice period in comparison with the lattice period of TiN coatings (Table 1).

3.3. High-entropy coatings

The next direction of research was to establish the features of the formation of multicomponent coatings to obtain a complete picture of the influence of alloying elements for further predictions and modeling of various types of coatings. When developing the concept of high-entropy alloys (HEAs), scientists are guided by the thermodynamic characteristics of the metal as a closed system and the influence of these characteristics on the structure and operational properties of the alloys. In particular, we are talking about the entropy of mixing ΔS_{mix} and the enthalpy of mixing ΔH_{mix} [24]. This makes it possible to predict with high accuracy the phase composition, stability and type of the crystal lattice of the alloy.

According to the Boltzmann equation, entropy of mixing is described by the expression:

$$\Delta S_{mix} = -R \sum_{i-1}^{n} c_i ln c_i \quad , \qquad (1)$$

where R is the universal gas constant (R = 8.314 J/mol·K), c_i is the concentration of the i-th element of the alloy.

An increase in the mixing entropy leads to a decrease in the Gibbs free energy of the alloy and, therefore, to an increase in the stability of the solid solution, according to the Gibbs equation:

$$\Delta G_{mix} = \Delta H_{mix} - T\Delta S_{mix} \quad , \qquad (2)$$

where ΔG_{mix} is the Gibbs potential; ΔH_{mix} is the enthalpy of mixing; T is the temperature.

Based on literature data, S_{mix} for HEA is usually in the range of 12 – 19 J/mol·K. Due to the high configurational entropy of mixing, HEAs are usually solid solutions with an fcc or bcc crystalline lattice. However, in order to

avoid the appearance of other phases, such as intermetallic compounds, Laves phases, amorphous phases, and others, the Ω-parameter theory was developed [25]. The Ω parameter is defined by the expression:

$$\Omega = \frac{T_m \Delta S_{mix}}{\left| \Delta H_{mix} \right|} \qquad (3)$$

Here T_m is the melting temperature of the alloy, which can be determined by the expression:

$$T_m = \sum_{i-1}^{n} c_i (T_m)_i \qquad (4)$$

where $(T_m)_i$ is the melting temperature of the i-th element of the alloy.

The enthalpy of mixing (ΔH_{mix}) of the alloy is determined by the formula:

$$\Delta H_{mix} = \sum_{i=1, j \neq i}^{n} \Omega_{ij} c_i c_j \quad , \qquad (5)$$

where Ω_{ij} is the parameter of each pair of alloy elements calculated according to the expression:

$$\Omega ij = 4\Delta H_{mix}^{AB} \quad , \qquad (6)$$

where ΔH^{AB}_{mix} is the mixing enthalpy of the AB binary alloy. This parameter can be calculated using Miedema's formulas and model [26].

Another important parameter for the formation of VEA is the parameter that takes into account the difference in the atomic radii of the alloy elements. [27]. It is described by the expression:

$$\delta = 100 \sqrt{\sum_{i-1}^{n} c_i (1 - r_i / r)^2} \quad , \qquad (7)$$

where n is the number of elements in the alloy; c_i is the concentration of the i-th element; r_i is the atomic radius of the i-th element [28]; r is the the average atomic radius of the alloy.

$$\bar{r} = \sum_{i=1}^{n} c_i r_i . \qquad (8)$$

According to [27, 29, 30], HEA are able to form solid solutions without intermetallic compounds and an amorphous phase at $\Omega \geq 1.1$ and $\delta \leq 6.6$. When the conditions –15 kJ/mol < ΔH_{mix} < 5 kJ/mol and $\delta \leq 4.6$ are met, a disordered solid solution is formed.

Another important parameter determining the phase stability and phase composition of HEA is the concentration of valence electrons (VEC) [27, 29, 30]. VEC is defined by the expression:

$$VEC = \sum_{i=1}^{n} c_i (VEC)_i \qquad (9)$$

Table 3 – Elemental composition of the initial targets

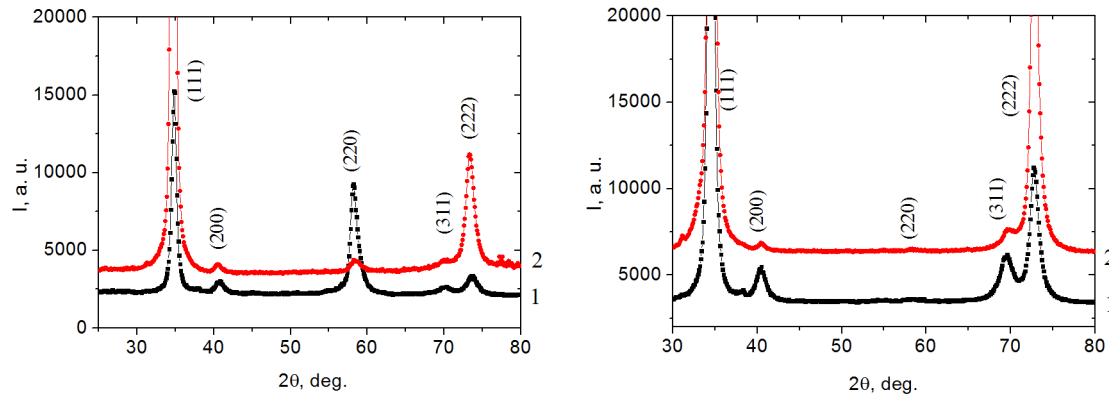| Sample	Concentration of elements, at. %					
	Ti	V	Zr	Nb	Hf	Ta
1 (TiVZrNbHf)	30.22	5.78	26.42	22.58	15	-
2 (TiVZrNbHfTa)	13.73	5.21	22.75	22.33	21.96	14.02

Fig. 3. XRD patterns of (TiVZrNbHf)N (a) and (TiVZrNbHfTa)N (b) coatings obtained at $U_c = -200$ V: 1 − $p_N = 0.26$ Pa; 2 − $p_N = 0.66$ Pa

where $(VEC)_i$ is the valence electron concentration of the i-th element.

As noted in [29], when VEC ≥ 8, a single fcc phase is formed in the alloy; in the range $6.87 \leq$ VEC ≤ 8, a mixture of fcc and bcc phases is present in the alloy; at VEC<6.87, only one phase with a bcc lattice is present in the alloy.

On the basis of the given theory, the parameters ΔH_{mix}, ΔS_{mix}, δ, VEC and Ω for HEA Ti-V-Zr-Nb-Hf and Ti-V-Zr-Nb-Hf-Ta with various compositions indicated in Table 3 were calculated. Table 3 shows elemental compositions of the initial targets used for (TiVZrNbHf)N and (TiVZrNbHfTa)N coatings. Table 4 shows the atomic radii and concentrations of valence electrons for elements in the TiVZrNbHfTa alloy. Table 5 shows the values of mixing enthalpy of binary alloys containing the elements of TiVZrNbHfTa HEA, obtained by calculations according to Miedema's model [31]. Table 6 shows the calculated values of parameters ΔH_{mix}, ΔS_{mix}, δ, VEC and Ω for TiVZrNbHfTa alloys of different compositions.

According to the results of the calculations, it follows that alloys 1 and 2 (compositions are indicated in Table 3) are indeed high-entropy according to the criteria specified in [27, 29, 30]. The conditions specified in these works are also met: Ω ≥ 1.1 at δ ≤ 6.6 and -15 kJ/mol $< \Delta H_{mix} < 5$ kJ/mol, which are necessary for the formation of a disordered solid solution without intermetallic and amorphous phases. From Table 6, VEC<6.87 for both alloy compositions 1 and 2, which indicates that only one phase with bcc

crystal lattice will be present in the alloy. Based on the analysis of literature data [24-31] and the performed calculations, it can be assumed that when using targets made of VEA 1 and 2 alloys with a bcc lattice, single-phase coatings with an fcc crystal lattice will be formed.

Experimental studies were carried out to confirm the theoretical model. Sections of X-ray diffraction spectra from (TiVZrNbHf)N and (TiVZrNbHfTa)N coatings are shown in Fig. 3 a, b, respectively.

Vacuum-arc evaporation (residual atmospheric pressure 0.0066 Pa) of targets from high-entropy systems Ti-V-Zr-Nb-Hf and Ti-V-Zr-Nb-Hf-Ta with element contents close to equiatomic, led to the formation of a single-phase coatings with fcc crystal lattices. The parameters of the crystal lattices were 0.4429 nm and 0.4448 nm, respectively, a strong texture with the [111] axis parallel to the direction of incidence of the film-forming particles was detected. The larger lattice period in the unstrained cross section for (TiVZrNbHfTa)N is associated with a larger content of elements with large atomic radii. At the same time, the macrostrain noticeably increases with increasing nitrogen pressure for alloys 1 and 2 (Fig. 4).

If we compare the diffraction spectra for five- and six-element nitride coatings, it is clear that the introduction of a sixth strong nitride-forming element leads to increased texture formation with a preferential crystallite orientation (111). At the same time, the texture (220) does not occur in the entire pressure range.
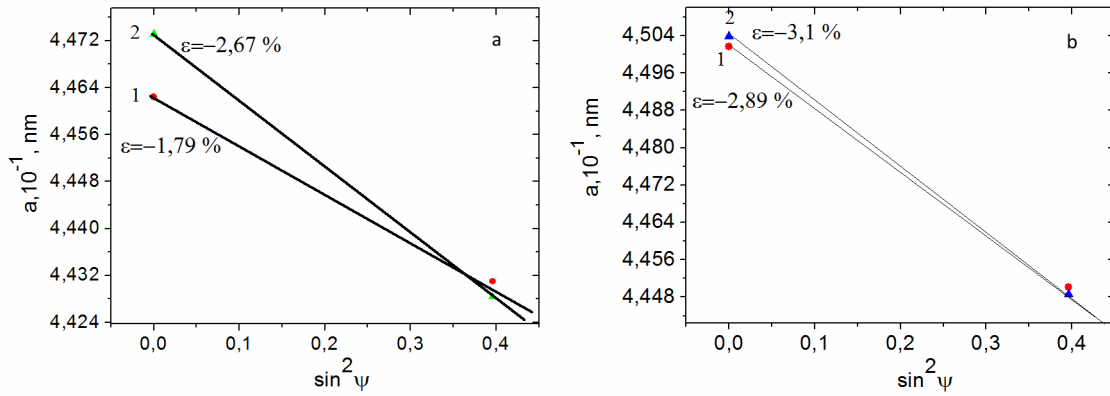
Fig. 4. "$a - \sin^2\psi$" graphs for HEAs (TiVZrNbHf)N (a) and (TiVZrNbHfTa)N (b): $1 - p_N = 0.26$ Pa; $2 - p_N = 0.66$ Pa

Table 5 – The value of ΔH^{AB}_{mix} calculated in the Miedema model of dual alloys [31, 32]

Element	Entropy of displacement of elements ΔH^{AB}_{mix}, kJ/mol				
	V	Zr	Nb	Hf	Ta
Ti	−2	0	2	0	1
V	–	–	−1	–	−1
Zr	–	–	4	–	−3
Nb	−1	4	–	–	0
Hf	−2	0	4	–	–
Ta	−1	−3	0	–	–

Table 4 – Atomic radius and concentrations of valence electrons in TiVZrNbHfTa alloy elements [24]

Element	Ti	V	Zr	Nb	Hf	Ta
Atomic radius, nm	0.147	0.134	0.162	0.146	0.158	0.149
VEC	4	5	4	5	4	5

It was established that with increasing pressure of the working nitrogen atmosphere, the content of the nitrogen component in the coating increases, up to the superstoichiometric content of 14.1 wt. % at the highest pressure of 0.66 Pa. The latter usually leads to some decrease in mechanical performance.

As an intermediate conclusion, it should be noted that with an excess of nitrogen (at the highest pressure of 0.66 Pa), the (111) texture is always formed, regardless of the composition and percentage of Hf.

As for the substructural characteristics, the introduction of the 6th heavy element (Ta) to the coating helps to reduce the average size of crystallite grains to 20-23 nm; this is especially noticeable at low pressures, where, due to the low loss of collision energy, particles are deposited with a relatively large average kinetic energy.

Therefore, it can be concluded that at low pressure, the main contribution to the development of microstrain is made by the particles accelerated in the bias potential field. At the same time, in the five-component system, the maximum value of microstrain is 1.1% at the bias potential of −200 V. The highest microstrain ($<\varepsilon> = 1.42\%$) is characteristic of a six-component coating at low pressure. High microstrains are typical for multicomponent systems in a single-phase state with a simple lattice. The reason is the difference in the atomic radii of the constituent components, which at low pressure bombard the growing coating with practically no energy loss.

At high pressure ($p_N = 0.66$ Pa), when the energy of the deposited particles drops sharply due to the collision in the gap between the cathode and the substrate, for all types of coatings (TiVZrNbHf)N and (TiVZrNbHfTa)N there is a

Table 6 – Values of parameters ΔH_{mix}, ΔS_{mix}, δ, VEC and Ω for TiVZrNbHf and TiVZrNbHfTa alloys

Alloy	ΔH_{mix}, kJ/mol	ΔS_{mix}, J/mol	δ	VEC	Ω
1	-0.23	1.7065	5.10	4.32	2.06
2	-0.21	1.4987	5.36	4.41	1.81

drop in microstrain of up to 0.7 % and 0.45% respectively.

As for mechanical properties, coatings obtained at a pressure of 0.26 Pa have the highest hardness value of 53–55 GPa. It should be noted that the higher hardness in the five-component system (H = 40 GPa) can be explained by the higher content of heavy Hf atoms.

Thus, the combination of elements in the system and technological deposition conditions play a major role in the formation of multicomponent coatings and final properties. Using the theoretical model, it is possible to estimate in advance the type of crystal lattice and the complex of properties, as well as select the composition of targets when planning an experiment. For all studied systems, the phases formed during deposition are characterized by nanosized crystallites (average size ~ 20 nm), thus, the synthesized coatings are nanocrystalline. At the same time, an increase in tantalum content leads to a decrease in the crystallite size (L) of the fcc phase due to the inhibition of diffusion processes with increasing distortion of the crystal lattice.

4. Conclusions

In coatings obtained by vacuum-arc reactive evaporation of a titanium target (in a nitrogen atmosphere), as a result of applying a constant negative bias, film-forming particles with increased energy lead to the formation of a single-phase TiN structure with a cubic lattice of the NaCl structural type. At a relatively high (–200 V) constant negative bias potential, a texture is formed [111]. The evolution of the observed texture can be associated with a change in the stress-strain state under the influence of a constant bias potential.

The addition of Mo to the coating does not significantly change the nature of the structure of the deposited coating. At the same time, the lattice period of TiMoN coatings increases slightly; this contributes to an increase in residual compressive stresses and, as a consequence, leads to an increase in hardness.

The study and development of this unique class of materials and the establishment of exact patterns of influence of the composition and deposition parameters on the final properties is an actual and rather promising task of modern solid state physics and materials science. It was established that the high entropy of

(TiVZrNbHf)N and (TiVZrNbHfTa)N systems stabilizes the formation of a single-phase system in the form of a disordered solid solution with an fcc lattice and prevents the formation of intermetallic compounds during the coating crystallization process. Coatings have a structure with the size of crystallites 20-23 nm. It was found that high-entropy coatings obtained at a nitrogen atmosphere pressure of 0.26 Pa and a constant bias potential of –200 V have the highest hardness values of 53–55 GPa. The theoretical model proposed for the analysis of the characteristics of high-entropy alloys and nitride coatings based on them has been confirmed experimentally.

References

1. D. Loktev, E. Ymashin, *Nanoindustry*, **4**, 18 (2007) [in Russian].
2. J. Musil, P. Baroch, P. Hard, *Research Singpost*, **1** (2008).
3. M.D. Drory, R.D. Evans, *Surf. Coat. Technol.*, **206**, 1983 (2011).
4. Sobol O.V., Pinchuk N.V. et al., *Functional Materials*, **27** (4), 736 (2020).
5. J. Lin, J. J.Moore, B. Mishra et al., *Acta Materialia*, **58**, 1554 (2010).
6. A.D. Pogrebnjak, I.V.Yakushchenko et al, *Materials Chemistry and Physics*, **147**, 1079 (2014).
7. Harish C. Barshilia, Shashidhara Acharya et al., Vacuum, 85, 411 (2010).
8. M.G.Faga, G.Gautier et al., *Wear*, **263**, 1306 (2007). – Vol.263. – P.1306-1314.
9. V.Riaboshtan, A. Zubkov et al., Lecture Notes in Mechanical Engineering, Grabchenko's International Conference on Advanced Manufacturing Processes, InterPartner, Odessa, Ukraine (2022), p. 334 – 342.
10. H.C. Barshilia, M. Ghosh, R. Ramakrishna, K.S. Rajam, *Applied Surface Science*, **256**, 6420 (2007).
11. G. Martinez et al., *Ceramics International*, **4**, 5757 (2014).
12. Li-Jian Meng, M.P. Santos, *Surface and Coatings Technology*, **90**, 64 (1997).
13. Az. Ahaitouf, J. C. Gerbedoen, A. Soltani, *J. Mater. Environ. Sci.*, **1**, 309 (2010).
14. Nadia, Karim Henda et Rafika Kesri, *J. Plasma fusion res. Series*, **8**, 1403 (2009).
15. M. F. Montemor, *Surface and Coatings Technology*, **258**, 17 (2014).

16. O.V. Sobol', A.A. Andreev, V.A. Stolbovoj, V.F. Grigor'ev, S.N. Volosova, S.V. Aleshin, V.F. Gorban', *VANT*, **4-98/74**, 174 (2011).

17. S.A. Firstov, V.F. Gorban, N.A. Krapivka, N.I. Danilenko, V.N. Nazarenko, *VANT*, **2** (96), 178 (2015).

18. Noyan I.C., Cohen J.B. Residual stress measurement by diffraction and interpretation, Springer-Verlag: NewYork, 1987; 350 p.

19. C. Genzel. *Phys. stat. sol. (a)* **159**, 283 (1997).

20. C. Genzel, W. Reinmers. *Phys. Stat. Solidi: A-Applied Research*, **166** (2), 751 (1998).

21. E. Aznakayev, Micron – Gamma for estimation the physico-mechanical properties of micro-materials, Proceedings of the International Conference "Small Talk – 2003", San Diego, California, USA (2003), p. 8-10.

22. V.F. Gorban', *Powder Metallurgy and Metal Ceramics*, **47** (7-8), 493 (2008).

23. F.F. Komarov, A.D. Pogrebnjak, S.V. Konstantinov, *Technical Physics*, **60** (10), 1519 (2015).

24. Jien Wei Yeh, Yu Liang Chen, Su Jien Lin, Swe Kai Chen, *Materials Science Forum*, **560**, 1 (2007).

25. P. Jinhong, P. Ye, *Rare Metal Materials and Engineering*, **42** (2), 232 (2013).

26. F. Tian, L.K. Varga, N. Chen, J. Shen, L. Vitos, *Intermetallics*, **58**, 1 (2015).

27. Y. Zhang, T. T. Zuo, Z. Tang, M.C. Gao, K.A. Dahmen, P.K. Liaw, Z.P. Lu, *Progress in Materials Science*, **61**, 1 (2014).

28. C.H. Lai, M.H. Tsai, S.J. Lin, J.W. Yeh, *Surface and Coatings Technology*, **201**, 6993 (2007).

29. Murty, B. S., Yeh J. W., Ranganathan S. High-Entropy Alloys, Elsevier: London, 2014; 213 p.

30. A.D. Pogrebnjak, A.A. Bagdasaryan, I.V. Yakushchenko, V.M. Beresnev, *Russ. chem. rev.*, **83** (11), 1027 (2014).

31. Akira Takeuchi, Akihisa Inoue, *Materials transactions*, **46** (12), 2817 (2005).

32. A.R Miedema; K.H.J Buschow; H.H Van Mal, *Journal of the Less-Common Metals*, **49**, 463 (1976).